

Joint RIS Assignment and Entanglement Distribution With Purification in FSO-Based Quantum Networks

Chun-An Yang^{§||}, Yung-Hsiang Chang^{†||}, Jing-Jhii Du[†], Juliette Chou Le Touze[†],
Jian-Jhii Kuo^{†*}, Chih-Yu Wang[‡], and Ming-Jer Tsai[§]

[§]Dept. of Computer Science, National Tsing Hua University, Hsinchu, Taiwan

[†]Dept. of Computer Science and Information Engineering, National Chung Cheng University, Chiayi, Taiwan

[‡]Research Center for Information Technology Innovation, Academia Sinica, Taipei City, Taiwan

Abstract—Ground-based free-space optical (FSO) quantum networks (QNs) have been regarded as a viable alternative to overcome the scalability and service availability limitations of fiber- or satellite-based QNs. However, FSO channels require line-of-sight connections between quantum access nodes (QANs) and user devices (UDs), making them highly susceptible to blockage by obstacles. Reconfigurable intelligent surfaces (RISs) have emerged as a promising solution by dynamically redirecting optical links to maintain connectivity. Despite their potential, RIS-assisted quantum transmissions pose challenges, including limited QAN capacity, fidelity degradation, UD demand requirements, and RIS assignments. To address these challenges, we formulate an optimization problem and propose a 2-approximation algorithm that jointly determines UD-RIS assignment and entanglement distribution while incorporating entanglement purification. Finally, simulation results demonstrate that our proposed algorithm outperforms existing baselines by at least 16%–38%.

Index Terms—ground-based FSO quantum network, reconfigurable intelligent surface, entanglement purification, approximation algorithm

I. INTRODUCTION

Quantum networks (QNs) have been validated to facilitate secure data transmission and quantum information processing [1], [2]. Most existing research on QNs has focused on fiber- or satellite-based architectures [3]–[5]. The former suffers from high deployment costs [6], and the latter faces challenges such as limited availability under adverse weather conditions and limited flexibility in dense urban environments [6]. To address these difficulties, recent studies have explored *ground-based free-space optical (FSO) QNs* [7], [8]. In this setting, ground quantum access nodes (QANs) generate and distribute entanglements to user devices (UDs), thereby enabling more reliable and adaptable entanglement distribution over moderate distances. Compared to wireline and non-terrestrial connections, ground-based FSO channels offer lower signal loss over similar distances and avoid the need for costly physical infrastructure [6], making them a promising option.

However, establishing communication paths for distributing entangled pairs inevitably involves long-distance transmission. Longer paths exacerbate decoherence effects and reduce the fidelity of entangled pairs. As the reduced fidelity does not meet the UDs' required fidelity thresholds, we can employ

||: equal contributions; *: corresponding author (lajacky@cs.ccu.edu.tw)

This work was supported in part by the National Science and Technology Council, Taiwan, under Grants 111-2221-E-007-044-MY3, 111-2628-E-194-001-MY3, 111-2628-E-001-002-MY3, 113-2221-E-194-040-MY3, 114-2628-E-194-002-MY3, 114-2221-E-001-017-MY2, 114-2221-E-007-079-, and 114-2218-E-194-001-.

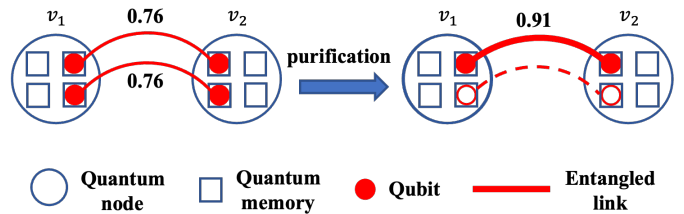


Fig. 1. An example of purification.

entanglement purification [1], [9], which consumes additional sacrificial entangled pairs to enhance the fidelity of target pairs. For clarity, Fig. 1 shows an example of purification, where the initial fidelity of an entangled pair ($\overline{v_1 v_2}$) is 0.76, below the required fidelity threshold of 0.8. A purification round is performed by consuming an additional sacrificial entangled pair (indicated by the dotted red line), improving the fidelity of ($\overline{v_1 v_2}$) to 0.91 and meeting the fidelity threshold. The purification can be applied repeatedly on the same target pair by progressively sacrificing more entangled pairs (i.e., resources) in each round until the fidelity threshold is satisfied.

Establishing FSO channels between the QAN and UDs still remains difficult, as line-of-sight (LoS) paths can be blocked by obstacles (e.g., buildings and trees). In addition, atmospheric turbulence can cause beam deflection, reducing the probability of successful entanglement distribution [6]. To address the LoS limitations in FSO-based QNs, recent studies have begun exploring the use of *reconfigurable intelligent surface (RIS)* into FSO-based QNs [10], [11], which have been shown to enhance spectral efficiency and link reliability in classical wireless communications by dynamically adjusting phase shifts of incoming optical waves at low energy cost [12]. Unlike active relays, RISs deployed in FSO-based QNs forward entangled pairs without requiring quantum memory, enabling cost-effective and low-latency entanglement distribution [11]. As shown in Fig. 2, we introduce an RIS-assisted FSO QN, in which generated entangled pairs can be delivered from the QAN to UDs on demand via intermediate RISs. It can be envisaged that RISs create virtual LoS paths to redirect optical signals and circumvent obstacles that block direct LoS paths, thereby improving service availability significantly.

The system aims to maximize the total weighted demand size by distributing entangled pairs to UDs with *all-or-nothing demand*—the fidelity and rate of entanglement pairs received by each UD must be fully satisfied, or such a requirement is con-

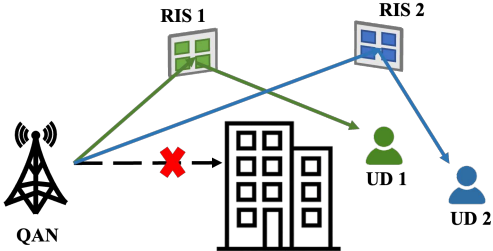


Fig. 2. Quantum network with RIS-assisted scheme.

sidered unmet—where each UD has a weight reflecting its priority. These factors lead to a non-trivial optimization problem, characterized by several fundamental challenges: 1) *Distance-fidelity trade-off under probabilistic success*. When transmission distances increase, especially through RIS-assisted paths, both the success probability of entanglement distribution and the fidelity of resulting entangled pairs decline exponentially. To meet the required fidelity thresholds, UDs with longer paths may require more entanglement purification rounds, consuming more entangled pairs. As a result, the system must carefully balance the trade-off between allocating resources to UDs suffering from reduced fidelity and preserving capacity to serve more UDs. 2) *Limited capacity versus all-or-nothing demand*. Each UD specifies an expected number of successfully established entangled links (i.e., a demand size), which must be fully satisfied. However, the QAN has a limited entanglement generation rate. Therefore, the allocation must balance resource consumption carefully to maximize the total demand size of satisfied UDs. 3) *Value-weighted resource allocation across multi-path options*. Each weighted UD has one or more paths from the QAN, each with a different cost and success probability. To address the trade-offs and constraints, we have to simultaneously assign RISs and distribute entangled pairs.

In the literature, the RIS assignment, entanglement distribution, and entanglement purification in QNs were solved separately [11], leading to suboptimal solutions.¹ To overcome these challenges, a new optimization problem is formulated to jointly consider UD-RIS association, entangled pair distribution, and entanglement purification under the conflicting and interdependent constraints, including QAN capacity, UD all-or-nothing demand (in terms of fidelity and rate), and RIS exclusivity constraint, where each RIS can serve at most one UD at a time. To the best of our knowledge, this is the first attempt in the literature to jointly consider all the above factors in RIS-assisted FSO-based QNs. The problem aims to maximize the total weighted demand size across all satisfied UD-RIS associations. To tackle this, a 2-approximation algorithm leveraging a tailored linear programming (LP) rounding technique is proposed. Simulation results show that the proposed algorithm outperforms existing baselines by at least 16% – 38%.

II. SYSTEM MODEL AND PROBLEM FORMULATION

A. System Model

We consider a ground-based FSO quantum network consisting of a QAN, a set of RISs $R = \{r_0, r_1, \dots, r_{|R|-1}\}$, and a

¹Due to the page limit, related works are summarized in Appendix A [13].

set of UDs $U = \{u_1, u_2, \dots, u_{|U|}\}$. For notation consistency, r_0 denotes a direct path from the QAN to a UD without using any RIS. The QAN can generate entangled pairs at a rate of $C \in \mathbb{R}^+$ and distribute them to each UD $u \in U$ through a selected path either directly r_0 or via the reflection of some RIS $r \neq r_0$. Each RIS $r \in R$ can serve at most one UD at the same time from its coverage $U_r \subseteq U$. The length of path (u, r) is denoted by $l(u, r)$, which includes both the QAN-to-RIS and RIS-to-UD segments if $r \neq r_0$, or the QAN-to-UD length if $r = r_0$. The success probability of distributing an entangled pair along path (u, r) follows an exponential decay model based on path length [14], i.e.,

$$\mathcal{P}_e(u, r) = e^{-\alpha \cdot l(u, r)}, \quad (1)$$

where α is a channel-dependent attenuation coefficient. The fidelity of the entangled pair over path (u, r) is assumed to follow the binary state and is modeled as [15]

$$\mathcal{F}_e(u, r) = \frac{1}{2} + \frac{1}{2} e^{-\beta \cdot l(u, r)}, \quad (2)$$

where β is a coefficient that captures decoherence effects, such as dephasing and detector imperfections [11], [16].

To improve the fidelity of low-quality entangled links, we apply entanglement purification [1], [9]. This process merges two entangled pairs with fidelity f_A and f_B , where one is treated as the target and the other as a sacrifice pair. The success probability of purification is given by [15]

$$\mathcal{P}_p(f_A, f_B) = f_A \times f_B + (1 - f_A) \times (1 - f_B). \quad (3)$$

Upon success, the resulting fidelity of the target pair becomes

$$\mathcal{F}_p(f_A, f_B) = \frac{f_A \times f_B}{f_A \times f_B + (1 - f_A) \times (1 - f_B)}. \quad (4)$$

In contrast, if purification fails, both input pairs are consumed.

To further improve the entanglement quality, we employ a recursive purification technique, *pumping* [1], [15], iteratively purifying a target entangled pair with multiple sacrifice pairs. Let $\mathcal{F}(u, r, n)$ be the fidelity of executing $n \in \mathbb{Z}_0^+$ rounds of pumping purification (using n sacrifice pairs) between the QAN and UD u via RIS r , and $\mathcal{P}(u, r, n)$ be the corresponding success probability. They can be respectively derived by

$$\mathcal{F}(u, r, n) = \mathcal{F}_p(\mathcal{F}(u, r, n-1), \mathcal{F}_e(u, r)), \quad (n \geq 1) \quad (5)$$

with the base case $\mathcal{F}(u, r, 0) = \mathcal{F}_e(u, r)$ and

$$\begin{aligned} \mathcal{P}(u, r, n) &= \mathcal{P}_p(\mathcal{F}(u, r, n-1), \mathcal{F}_e(u, r)) \\ &\quad \cdot \mathcal{P}(u, r, n-1), \quad (n \geq 1) \end{aligned} \quad (6)$$

with the base case $\mathcal{P}(u, r, 0) = 1$. Eqs. (5) and (6) present how fidelity and success probability are recursively calculated under the pumping technique, which obtains new results based on those from the preceding purification round.

Given a specific path (u, r) for UD $u \in U$, the minimum number of required input pairs to generate one purified entangled pair that meets the fidelity threshold $\mathcal{F}_{th}(u) \in \mathbb{R}^+$ is

$$n(u, r) = \arg \min_{n \in \mathbb{Z}_0^+} \{\mathcal{F}(u, r, n) \geq \mathcal{F}_{th}(u)\}. \quad (7)$$

Let $d(u)$ denote the expected number of successful entangled pairs per unit of time demanded by UD u . Satisfying the demand on path (u, r) requires the QAN to provide entangled pairs at a distribution rate of

$$s(u, r) = \frac{d(u)}{\mathcal{P}_e(u, r)} \cdot \frac{n(u, r) + 1}{\mathcal{P}(u, r, n(u, r))}. \quad (8)$$

Note that the UD's demand is satisfied only if the allocated rate equals or exceeds $s(u, r)$. Finally, each UD $u \in U$ is associated with a weight $w(u) \in \mathbb{R}^+$, reflecting its importance.

B. Problem Formulation – REAP

Following the above system model, we formulate the Joint RIS Assignment, Entanglement Distribution, and Purification Problem (REAP) as an integer linear programming (ILP). The goal is to jointly determine the UD-RIS assignment and entangled pair distribution such that the total weighted demand size between UDs and RISs is maximized. To this end, we define decision variable $x_{ur} \in \{0, 1\}$ indicating whether UD $u \in U$ is assigned to the path directly from the QAN or via RIS $r \in R \setminus \{r_0\}$. The REAP can be formulated as follows.

$$\max \sum_{r \in R} \sum_{u \in U_r} w(u) \cdot d(u) \cdot x_{ur} \quad (9a)$$

$$\text{s.t. } \sum_{r \in R} \sum_{u \in U_r} s(u, r) \cdot x_{ur} \leq C \quad (9b)$$

$$\sum_{r \in R: u \in U_r} x_{ur} \leq 1, \quad \forall u \in U \quad (9c)$$

$$\sum_{u \in U_r} x_{ur} \leq 1, \quad \forall r \in R \quad (9d)$$

$$x_{ur} \in \{0, 1\}, \quad \forall r \in R, \forall u \in U_r \quad (9e)$$

The objective (9a) maximizes the total weighted demand size for all satisfied UDs, ensuring that each satisfied UD can fully obtain the required entanglement rate in expectation. The constraint (9b) bounds the total distribution rate within the QAN capacity. The constraints (9c) and (9d) ensure that each UD is connected to at most one RIS, and each RIS serves at most one UD. Note that the NP-hardness of the REAP can be shown by introducing a polynomial-time reduction from a well-known NP-complete problem, the partition problem [17]. The detailed proof is in Appendix B [13] due to the page limit.

Theorem 1. The REAP is NP-hard.

III. ALGORITHM DESIGN – RELIC

A 2-approximation algorithm to the REAP, termed RELIC (Joint RIS Assignment and Entanglement Distribution With Purification Algorithm), is developed by applying LP relaxation followed by rounding. To achieve LP rounding, we first relax the binary variable x_{ur} in the ILP (9a)–(9e) to $x_{ur} \geq 0$ between each RIS $r \in R$ and each UD $u \in U_r$. Then, we add one more constraint $(C - s(u, r)) \cdot x_{ur} \geq 0, \forall r \in R, \forall u \in U_r$, ensuring that the QAN has sufficient capacity to fully serve UD u via RIS r if $x_{ur} > 0$. The relaxed LP can be solved in polynomial time by the existing LP solver (e.g., Gurobi). After acquiring the optimum LP solution, we then round it to

an integral solution. For ease of presentation, we define \tilde{x}_{ur} and $v(u)$ to denote the optimum LP solution and $w(u) \cdot d(u)$, respectively, in the following.

Intuitively, iteratively selecting the UD-RIS edge with the highest \tilde{x}_{ur} (i.e., rounding it to one) tends to yield a higher total weighted demand size. However, this naive approach may make some UD u have no edge even if $\sum_{r \in R: u \in U_r} \tilde{x}_{ur} = 1$ due to constraints (9b) and (9d). This will result in a huge gap to the optimum LP solution since such UDs are more preferable than others for the optimum LP solution. To identify such UDs, we define the *UD fulfillment level (UFL)* $L(u) = \sum_{r \in R: u \in U_r} \tilde{x}_{ur}$ to indicate the optimum LP solution's preference for each UD u ; it could be *fully served* (i.e., $L(u) = 1$), *partially served* (i.e., $L(u) \in (0, 1)$), and *unserved* (i.e., $L(u) = 0$). Subsequently, we consider only the fully and partially served UDs. Thus, we construct an auxiliary edge-weighted graph $\tilde{G} = (\tilde{U} \cup \tilde{R}, \tilde{E})$, where \tilde{U} represents all fully and partially served UDs, \tilde{R} includes all RISs r with $\sum_{u \in \tilde{U} \cap U_r} \tilde{x}_{ur} > 0$, and \tilde{E} denotes all the edges between UD $u \in \tilde{U}$ and RIS $r \in \tilde{R}$ with $\tilde{x}_{ur} > 0$. Also, the weight of each edge in \tilde{E} indicates the required distribution rate $s(u, r)$. In other words, \tilde{G} discards all the unserved UDs and zero-valued edges.

To design an efficient rounding method, we first introduce several key concepts that underpin our design. An *intra-transfer* operates on a cycle or a *maximal extended path* (Definition 1) formed by UD-RIS edges with positive values in the current solution \tilde{x} . Along such a structure, we may transfer the fractional value in either of two directions (referred to as *forward* and *backward*). We always select the direction that ensures $\Delta v = 0$ and $\Delta s \leq 0$ for the intra-transfer operation, where Δv and Δs denote the changes in the total weighted demand size and total distribution rate, respectively, after the transfer operation. By repeating the transfer such that some edges become integral (0 or 1), we gradually drive the solution closer to integrality, while preserving the total weighted demand size without increasing the total distribution rate.

Definition 1. A *maximal extended path* is identified by starting from any RIS in \tilde{G} and extending hop by hop in each direction. The extension stops as no further hop is possible or a partially served UD is encountered. Consequently, a maximal extended path contains at most two partially served UDs, and if such UDs exist, they must appear as the endpoints of the path.

However, not all paths admit such clean rounding. In certain cases, any intra-transfer would either increase or decrease both the total weighted demand size and distribution rate (i.e., either $\Delta v > 0, \Delta s > 0$ or $\Delta v < 0, \Delta s < 0$), failing to make progress toward integrality. We refer to such structures as *intra-locked paths*. To handle intra-locked paths, we couple two of them and perform an *inter-transfer*, adjusting the transfer amounts on the two paths so that their combined effect preserves total weighted demand size (i.e., $\Delta v = 0$). Since there are two orientations (i.e., transferring from path 1 to path 2 or vice versa), at least one orientation ensures that the resulting change in distribution rate satisfies $\Delta s \leq 0$. Through repeated intra- and inter-transfers, most fractional edges can be eliminated, leaving at most one intra-locked path. To address this, we select

a specific UD from \tilde{U} as the *pivot* and derive two candidate solutions using the minimum weight matching algorithm and a customized greedy strategy, respectively; the first candidate does not include the pivot, while the second one does.

Specifically, the partially served UD $u \in \tilde{U}$ that has an edge $(u, r) \in \tilde{E}$ with the highest $s(u, r)$ is chosen as the pivot, i.e.,

$$p = \arg \max_{u \in \tilde{U}: L(u) \in (0,1)} \left(\max_{r \in \tilde{R}: (u, r) \in \tilde{E}} s(u, r) \right). \quad (10)$$

The first candidate solution includes all the UD-RIS edges selected in the minimum weight matching (using $s(u, r)$ as weights) for the subgraph of \tilde{G} , extracted by removing the pivot p and p 's incident edges from \tilde{G} . Afterward, the second candidate using a customized greedy strategy first selects the edge between the pivot p and its RIS with the highest $s(p, r)$ and then iteratively selects the UD-RIS edges included in the first candidate with the highest ratio of $\frac{v(u)}{s(u, r)}$, referred to as the *cost-efficiency index (CEI)*, until the QAN capacity runs out. Finally, we choose the candidate with a higher total weighted demand size as well as the UD-RIS edges selected during the intra- and inter-transfer operations as the final solution.

The proposed RELIC comprises two main phases: 1) Fractional Solution Transfer (FST) and 2) Final Solution Generation (FSG). The FST performs transfer operations to round some \tilde{x}_{ur} values to 0 or 1. The FSG generates two candidate solutions for the last intra-locked path with partially served UDs if needed. Then, the candidate with a larger weighted demand size is selected. The following subsections detail the two phases using illustrative examples.

A. Fractional Solution Transfer (FST)

After obtaining the optimum LP solution, the FST constructs the auxiliary graph $\tilde{G} = (\tilde{U} \cup \tilde{R}, \tilde{E})$, where the nodes and edges are the fully and partially served UDs and their edges with $\tilde{x}_{ur} > 0$, respectively. First, all UD-RIS edges with $\tilde{x}_{ur} = 1$ are fixed into the rounded solution and removed from \tilde{G} . The FST then iteratively explores \tilde{G} using depth-first search (DFS) from any RIS to locate a cycle or a maximal extended path. On each identified structure, a small fraction of the assignment is shifted between even edges and odd edges; the direction with $\Delta v = 0$ and $\Delta s \leq 0$ is always chosen, and edges updated to 0 or 1 are fixed accordingly. When a path cannot be resolved by intra-transfer alone, the FST performs inter-transfer by pairing it with another unresolved path and adjusting the transfer amounts so that $\Delta v = 0$ and $\Delta s \leq 0$. This procedure continues until no further intra- or inter-transfer can be applied.

Fig. 3 illustrates an example of the intra-transfer operation. Each edge between a fully served UD and an RIS is labeled with its fractional value \tilde{x}_{ur} . In Fig. 3(a), UD u_1 is fully served by RIS r_1 with $\tilde{x}_{u_1 r_1} = 1$ and is thus excluded from further processing. The DFS is then performed to identify a maximal extended path as shown in Fig. 3(b). The transfer operation that yields a lower total distribution rate is chosen. In this case, the values $\tilde{x}_{u_2 r_3}$ and $\tilde{x}_{u_3 r_2}$ of the odd edges (u_2, r_3) and (u_3, r_2) , both equal to 0.46, are rounded down to 0, while the two even edges' values $\tilde{x}_{u_2 r_2}$ and $\tilde{x}_{u_3 r_4}$, both equal to 0.54, are rounded up to 1. After this operation, all UDs are satisfied by a single edge. The resulting UD-RIS assignment is shown in Fig. 3(c).

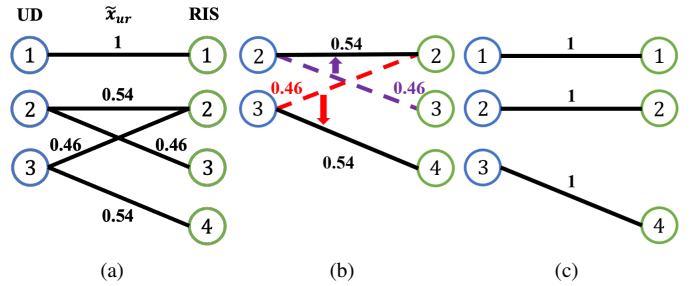


Fig. 3. An example of intra-transfer operation.

B. Final Solution Generation (FSG)

When only one intra-locked path remains (i.e., the case of either $\Delta v < 0, \Delta s < 0$ or $\Delta v > 0, \Delta s > 0$), the FSG resolves it by generating two candidate solutions with respect to a pivot p . The partially served UD that has an edge $(u, r) \in \tilde{E}$ with the maximum distribution rate $s(u, r)$ is chosen as the pivot p . To construct the first candidate solution, the FSG builds a bipartite matching instance where the UDs and RISs form the two sides of the bi-partition, and each UD-RIS edge (u, r) is assigned a weight equal to its distribution rate $s(u, r)$. Running the Hungarian algorithm [18] on this instance yields the minimum weight matching, which serves as the first candidate solution. Fig. 4(a)–4(c) show an example of the first candidate solution, with each edge's \tilde{x}_{ur} value listed in Table I. The total weighted demand and distribution rate of the optimum LP solution are 18.4 and 30, respectively. If the fraction is transferred from the black edges to the orange edges, thereby moving the solution toward using only orange edges, the total weighted demand and distribution rate become 17 and 18, respectively (i.e., intra-locked path). Since UD u_4 has the highest $s(u, r) = 20$, it is elected as p . The remaining edges (without p) in Fig. 4(b) are then processed using the Hungarian algorithm [18] to obtain the UD-RIS assignment with the minimum total distribution rate. The first candidate solution is shown in Fig. 4(c).

The FSG generates the second candidate solution including the pivot p . Specifically, the selected edges from the first candidate solution are sorted in non-increasing order of their CEIs. The edge between pivot p and its RIS r with the highest $s(p, r)$, along with the sorted edges, are sequentially included until the QAN capacity runs out. Last, we select the candidate solution with a higher total weighted demand size as part of the final solution. In Fig. 4(d), UD u_4 is selected as p and its incident edge (p, r) is added to the second candidate solution. The selected edges from the first candidate solution, as shown in Fig. 4(c), are then sorted in descending order of their CEIs. Specifically, edges (u_1, r_1) , (u_3, r_2) , and (u_2, r_3) have CEIs of $\frac{5}{3}$, $\frac{6}{5}$, and $\frac{6}{10}$, respectively, satisfying the order $\frac{5}{3} > \frac{6}{5} > \frac{6}{10}$. After selecting edges (u_1, r_1) and (u_3, r_2) , the total distribution rate reaches 28, which would exceed the capacity if edges (u_2, r_3) were also selected. The second candidate solution is shown in Fig. 4(d), where the total weighted demand size is 18. Finally, the second candidate is adopted as the final solution since it has a higher total weighted demand size than the first one. Note that the RELIC is a 2-approximation algorithm. Due to the page limit, the proof is detailed in Appendix C [13].

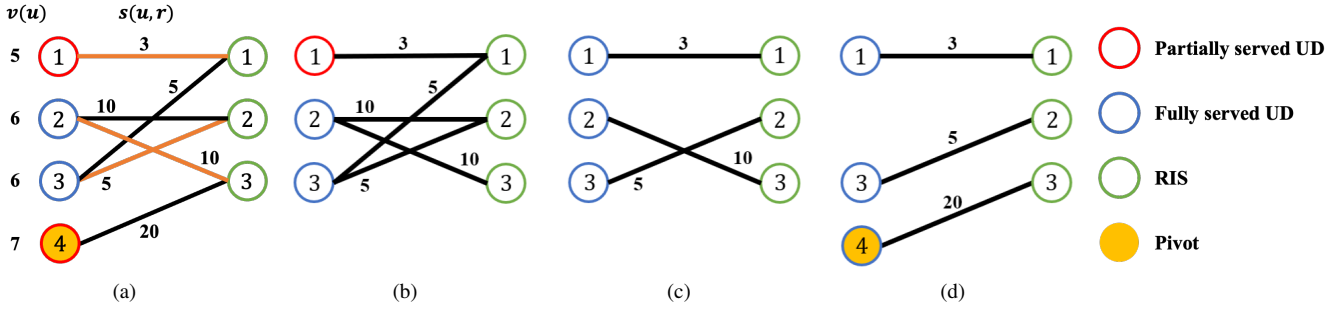


Fig. 4. An example of intra-locked path, where $C = 30$.

TABLE I
VALUE OF \tilde{x}_{ur}

	$\tilde{x}_{u_1r_1}$	$\tilde{x}_{u_2r_2}$	$\tilde{x}_{u_2r_3}$	$\tilde{x}_{u_3r_1}$	$\tilde{x}_{u_3r_2}$	$\tilde{x}_{u_4r_3}$
Value	0.3	0.7	0.3	0.7	0.3	0.7

Theorem 2. The RELIC is a 2-approximation algorithm.

IV. PERFORMANCE EVALUATION

A. Simulation Settings

1) *Network Scenarios:* We generate multiple 1600×1600 m² 3D grid networks, each with a QAN deployed at coordinates (0, 0, 90) m and several UDs randomly scattered following a truncated normal distribution. Particularly, each UD u is placed at coordinates $(x_u, y_u, 10)$ m, where $x_u \sim \mathcal{T}\mathcal{N}(250, 50, 50, 1650)$ m and $y_u \sim \mathcal{T}\mathcal{N}(200, 50, 0, 1600)$ m. Then, we randomly deploy each RIS r at coordinates (x_r, y_r, z_r) m within a cuboid, where $x_r \in [50, 1650]$, $y_r \in [0, 1600]$, $z_r \in [35, 90]$. We assign a random orientation angle $\phi_r \in [0, 2\pi]$ for each RIS to indicate the direction of its surface normal. Note that serving a UD requires that the RIS's effective reflection sector, denoted by $[\phi_r - \frac{\theta}{2}, \phi_r + \frac{\theta}{2}]$, covers the UD, where $\theta = 180^\circ$ according to [19].

2) *Parameter Settings:* The number of UDs and RISs are set to 50 and 15, respectively. Following [11], we set the limited QAN capacity to 10^7 pairs per unit of time. Each UD specifies an expected number of successful entangled links per unit of time, randomly selected from $[10^5, 10^6]$. The probability of successful entanglement and the initial entangled fidelity are computed using Eqs. (1) and (2), with the parameters $\alpha = 0.4$ and $\beta = 1.2$ (1/km) obtained by fitting the experimental data reported in [11]. The required fidelity threshold for each UD is randomly drawn from a uniform distribution over $[0.7, 0.9]$ [20]. As suggested in [21], the willingness to pay (WTP) of each UD is mapped to a weight $w(u)$. The limited availability of entangled pairs naturally creates competition among UDs. Auction theory [22] indicates that bidding behaviors can often be approximated by a normal distribution. Following this insight, we generate WTP values by drawing samples from a normal distribution with median 1 and standard deviation 1.5, taking only the positive half, and then scaling them into the normalized interval $[1, 3]$. In this formulation, the weight assigned to a UD reflects its WTP, ensuring that larger WTP values lead to proportionally greater weights.

3) *Baselines:* The performance of the proposed RELIC is compared with four baselines. 1) **Ratio-based Greedy (RG):**

assigns UDs to RISs in weakly decreasing order of CEIs until the QAN capacity runs out. 2) **Value-based Greedy (VG):** selects UDs by non-increasing order of $v(u)$ and assigns it to the RISs with the lowest $s(u, r)$ until it exhausts the QAN capacity. 3) **Simulated Annealing (SA):** assigns UDs to RISs using the metaheuristic [11]. 4) **OPT:** calculates the optimal solution of ILP (9a)–(9e) via Gurobi. Note that each simulation result is obtained by averaging over 100 trials.

B. Numerical Results

Fig. 5 shows the performance changes over different parameters. The RELIC optimizes UD-RIS association together with entangled pair distribution and purification, aiming to maximize the total weighted demand size and surpassing other baselines. We then explain the results in detail as follows.

1) *Effect of Numbers of UDs/RISs:* Fig. 5(a)–5(d) illustrate the impact of varying numbers of UDs/RISs on the total weighted demand size, total distribution rate, and number of satisfied UDs. Fig. 5(a) shows that enlarging the UD set mildly increases the total weighted demand size, owing to the greater probability of selecting higher-value users. However, Fig. 5(b) exhibits no clear increasing or decreasing trend in the total distribution rate. This is because most methods, except for the SA, tend to fully utilize the available capacity, as the resources are relatively scarce. Subsequently, Fig. 5(c) demonstrates that the total weighted demand size increases with the number of RISs, as more RISs enable the system to serve a greater number of UDs (as shown in Fig. 5(d)). As a result, the RG preferring high-CEI UD-RIS assignment misses high- $v(u)$ UDs, the VG prioritizing high- $v(u)$ UDs neglects CEI, and the SA fails to consider purification, leading to worse performance. In contrast, our proposed RELIC can achieve a higher total weighted demand size close to the OPT through effective UD-RIS assignment, while maintaining efficient rate distribution, thus successfully mitigating the second and third challenges.

2) *Effect of QAN capacity:* Fig. 5(e) and 5(f) present how the total weighted demand size and the total distribution rate evolve with increasing QAN capacity. A larger capacity allows the QAN to serve more UDs, providing more flexibility in RIS assignment and resource allocation. Compared to the other methods, our RELIC can efficiently distribute the additional available resources by selecting more valuable UD-RIS assignments to satisfy UD demands, leading to a higher total weighted demand size and addressing the second challenge.

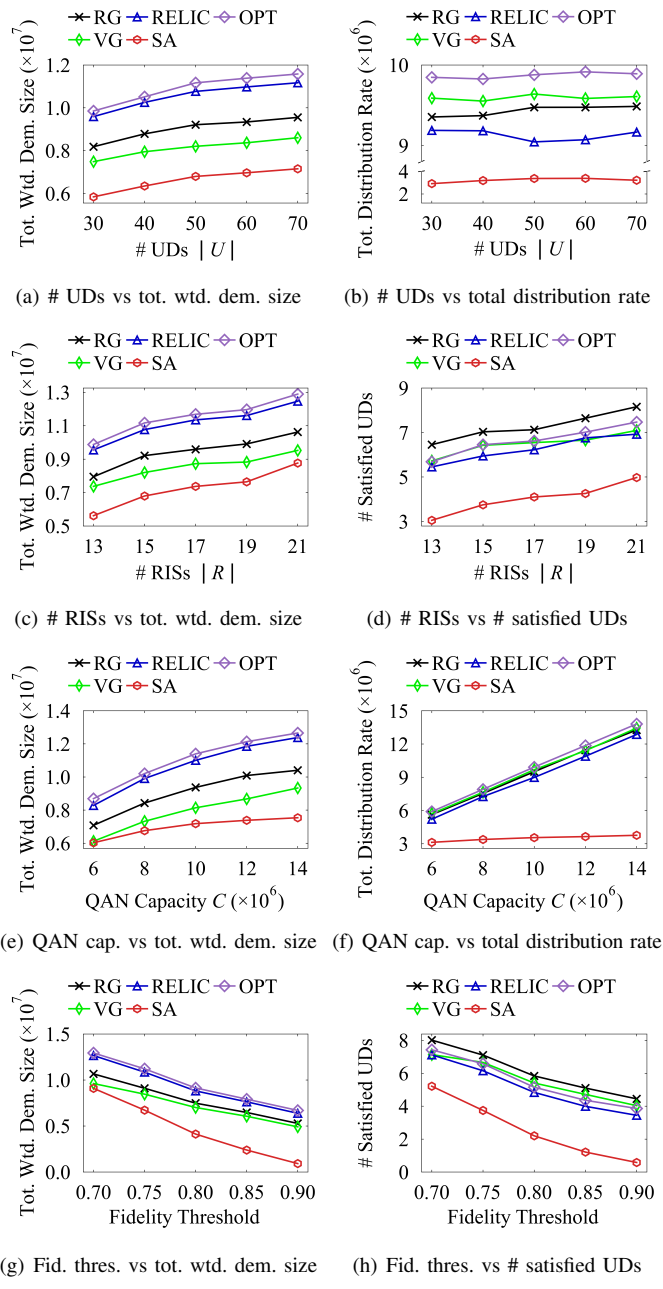


Fig. 5. Effects of different parameters on different metrics.

3) *Effect of Fidelity Threshold:* Fig. 5(g) and 5(h) display the values of the total weighted demand size and the number of satisfied UD under the effect of different ranges of fidelity threshold. For each experiment, the individual fidelity threshold of each UD is randomly sampled from a uniform interval $[f_{\min}, f_{\min} + 0.05]$, where $f_{\min} \in \{0.65, 0.7, 0.75, 0.8, 0.85\}$ represents the lower bound of the tested range. As the fidelity threshold increases, the required number of purification rounds also escalates. In contrast to other algorithms, without implementing purification, the SA fails to meet most fidelity requirements, resulting in a drastic drop in both the demand size and the satisfied UD. Compared to all the other algorithms, our proposed RELIC achieves a higher total weighted demand size close to the OPT, efficiently solving the first challenge.

V. CONCLUSION

In this work, we address an optimization problem termed REAP, where UD-RIS association, entangled pair distribution, and purification are determined jointly to maximize the total weighted demand size for all UD. To this end, we propose a 2-approximation algorithm named RELIC with two phases: FST and FSG. The FST nearly rounds all fractional edges away through intra- and inter-transfers. If only one resistant path (i.e., an intra-locked path) remains, the FSG steps in; by choosing a pivot, generating two candidate solutions, and selecting the better one, it neatly resolves what transfers alone cannot handle. The two phases guide the QAN in establishing entangled links with UD via selected RISs. Simulation results show that the RELIC outperforms the other baselines by at least 16%–38%.

REFERENCES

- [1] R. Van Meter, *Quantum Networking*. John Wiley & Sons, Ltd, 2014.
- [2] S. Shi and C. Qian, “Concurrent entanglement routing for quantum networks: Model and designs,” in *ACM SIGCOMM*, 2020.
- [3] M. Chehimi *et al.*, “Entanglement rate optimization in heterogeneous quantum communication networks,” in *ISWCS*, 2021.
- [4] Y.-A. Chen *et al.*, “An integrated space-to-ground quantum communication network over 4,600 kilometres,” *Nature*, vol. 589, no. 7841, pp. 214–219, 2021.
- [5] L. Mazzarella *et al.*, “QUARC: Quantum research cubesat—a constellation for quantum communication,” *Cryptography*, vol. 4, no. 1, p. 7, 2020.
- [6] N. Hosseiniidehaj *et al.*, “Satellite-based continuous-variable quantum communications: State-of-the-art and a predictive outlook,” *IEEE Commun. Surv. Tutorials*, vol. 21, no. 1, pp. 881–919, 2019.
- [7] H. Zhao and M.-S. Alouini, “On the transmission probabilities in quantum key distribution systems over FSO links,” *IEEE Trans. Commun.*, vol. 69, no. 1, pp. 429–442, 2021.
- [8] A. Dhiman *et al.*, “Classical-quantum signaling via stokes parameters,” in *IEEE GLOBECOM*, 2024.
- [9] J.-W. Pan *et al.*, “Entanglement purification for quantum communication,” *Nature*, vol. 410, pp. 1067–1070, 2001.
- [10] N. K. Kundu *et al.*, “Intelligent reflecting surface-assisted free space optical quantum communications,” *IEEE Trans. Wirel. Commun.*, vol. 23, no. 5, pp. 5079–5093, 2024.
- [11] M. Chehimi *et al.*, “Reconfigurable intelligent surface (RIS)-assisted entanglement distribution in FSO quantum networks,” *IEEE Trans. Wirel. Commun.*, vol. 24, no. 4, pp. 3132–3148, 2025.
- [12] M. Jung *et al.*, “Performance analysis of large intelligent surfaces (LISs): Asymptotic data rate and channel hardening effects,” *IEEE Trans. Wirel. Commun.*, vol. 19, no. 3, pp. 2052–2065, 2020.
- [13] C.-A. Yang *et al.*, “Joint RIS assignment and entanglement distribution with purification in FSO-based quantum networks (appendix),” Apr 2025. [Online]. Available: <https://reurl.cc/ZNNrKM>
- [14] G. Zhao *et al.*, “Segmented entanglement establishment with all-optical switching in quantum networks,” *IEEE/ACM Trans. Netw.*, vol. 32, no. 1, pp. 268–282, 2024.
- [15] N. K. Panigrahy *et al.*, “On the capacity region of a quantum switch with entanglement purification,” in *IEEE INFOCOM*, 2023.
- [16] T. van Leent *et al.*, “Long-distance distribution of atom-photon entanglement at telecom wavelength,” *Phys. Rev. Lett.*, vol. 124, p. 010510, 2020.
- [17] D. P. Williamson and D. B. Shmoys, *The Design of Approximation Algorithms*. Cambridge University Press, 2011.
- [18] H. W. Kuhn, “The Hungarian method for the assignment problem,” *Nav. Res. Logist. Q.*, vol. 2, no. 1-2, pp. 83–97, 1955.
- [19] E. Björnson *et al.*, “Reconfigurable intelligent surfaces: A signal processing perspective with wireless applications,” *IEEE Signal Process. Mag.*, vol. 39, no. 2, pp. 135–158, 2022.
- [20] S. Massar *et al.*, “Optimal extraction of information from finite quantum ensembles,” *Phys. Rev. Lett.*, vol. 74, pp. 1259–1263, 1995.
- [21] Y. Lee *et al.*, “Quantum network utility: A framework for benchmarking quantum networks,” *Proc. Natl. Acad. Sci.*, vol. 121, no. 17, p. e2314103121, 2024.
- [22] V. Krishna, *Auction Theory*, 2nd ed. San Diego: Academic Press, 2009.